Artwork Imaging from 370 to 1630 nm Using a Novel Multispectral System Based on Light-Emitting Diodes

Jorge Herrera-Ramirez,[1]* Meritxell Vilaseca,[1] Francisco J. Burgos,[1] Lídia Font,[2] Rosa Senserrich,[3] Jaume Pujol[1]

[1]Centre for Sensors, Instruments and Systems Development (CD6), Universitat Politècnica de Catalunya (UPC), Terrassa, Barcelona, Spain

[2]Museum of Barcelona (MUHBA), Barcelona, Spain

[3]Faculty of Fine Arts, University of Barcelona, Barcelona, Spain

Received 15 March 2014; revised 10 July 2014; accepted 20 July 2014

Abstract: The recent use of multispectral systems as a noncontact method for analysis of artworks has already shown promising results. This study explains the application of a novel portable multispectral system based on light-emitting diodes (LEDs) for artwork imaging. This method provides spectral information in a spectral range from 370 to 1630 nm with a 25 cm × 25 cm field of view by using two different image sensors in synchrony with 23 bands of irradiation. The spectral information for each point is estimated and validated using the pseudo-inverse and spline interpolation methods for spectral estimation and three different evaluation metrics. The results of the metrics obtained with both estimation methods show a general good performance of the system over the whole spectral range. The experiments also showed that the selection of the training set for the pseudo-inverse estimation has a great influence in its performance, and thus, it defines whether or not the pseudo-inverse outperforms the spline interpolation method. The system is applied in situ to the study of Catalan art masterpieces, and the results demonstrate the potential of a cost-effective and versatile system using various off-the-shelf elements to reconstruct color information and to reveal features not previously identified. © 2014 Wiley Periodicals, Inc. Col Res Appl, 00, 000–000, 2014; Published Online 00 Month 2014 in Wiley Online Library (wileyonlinelibrary.com). DOI 10.1002/col.21910

Key words: art imaging; multispectral system; reflectance; light-emitting diodes

INTRODUCTION

Spectral imaging technology has evolved significantly during the past four decades. Based on the increase in the number of spectral bands and the reduction of spacing between them, new terms such as multispectral, hyperspectral, and ultraspectral imaging define different types of spectral imaging technology.[1] The impact of the rapid development of semiconductors and related technologies has substantially influenced today's numerous applications for spectral imaging. Although this technology was initially restricted to astrophysics, remote sensing, and terrestrial military applications,[2] it is currently found in such diverse areas as medicine, biometrics, environmental sciences, color technology, pharmacology, food engineering, and agriculture.[3–8]

Recently, some features of spectral image acquisition have been investigated for cultural heritage purposes.[9] First, access to spectral reflectance provides a more accurate color reproduction, thus avoiding dependence on illumination and acquisition devices.[10] These properties have facilitated processes of digital archiving and reproduction

*Correspondence to: Jorge Herrera-Ramirez (e-mail: jaherrer@gmail.com)

Contract grant sponsor: Spanish Ministry of Science and Innovation; contract grant numbers: DPI2008-06455-C02-01, DPI2011-30090-C02-01; Contract grant sponsors: European Union and Generalitat (Government) of Catalonia; Contract grant sponsor: European Cooperation in Science and Technology (COST); contract grant number: COST-action TD 1201: Colour and Space in Cultural Heritage (COSCH).

of collections.[11] Second, with the use of spectral imaging, the information obtained is objective, repeatable, and does not change over time, which allows monitoring of artworks conservation status. Third, spectral imaging permits material identification. Furthermore, data from nonvisible spectral ranges can provide important information, for example, infrared (IR) reflectography and ultraviolet (UV) luminescence provide insight into the history of the artwork, the artist's methods, and serve as a tool of conservation status diagnosis. In addition, spectral features of the materials can be drawn from the nonvisible parts of the spectrum.[12,13] Some of these tasks have been performed using other tools such as analytical chemical techniques developed for the identification of materials. However, techniques such as scanning electron microscopy, chromatography, and polarization microscopy require the extraction of a small sample; other techniques such as X-ray fluorescence spectroscopy, Raman spectroscopy, or fiber optic reflectance spectroscopy (FORS) can be used in situ, but they are all point measurement techniques, that is, based on a selection of points generally determined by visual inspection. Although some of these techniques such as FORS can scan the whole surface of the painting, they require long times of acquisition, rendering them impractical in most cases. In contrast, in situ spectral imaging systems can provide entire paint acquisition and depending on the specific implementation they can also guide the site selection for further study with point measurement methods.

There are various types of multispectral imaging systems, mainly single-point spectrometers with 2D scanning systems,[14] digital cameras combined with line scan or pushbroom spectrographs,[5] color filter wheels,[15–17] filter mosaics,[18] lenslet arrays together with narrowband filters,[19,20] and tunable filters of liquid crystal or acousto-optic technology.[21,22] Operational speed, spectral and spatial resolutions, and cost vary in each system, but they all use a light source with a wide spectral range of emission, such as a halogen or mercury–xenon lamp. By contrast, the current development of light-emitting diode (LED) technology has ameliorated wavelengths availability, efficiency, emission power, life cycle, and is in constant evolution. The LED elements offer narrow spectral emissions in wavelengths from the UV to the IR spectral ranges. They enable irradiating with specific wavelengths and customized combinations of wavelengths fast and in switching synchrony with the imaging sensors. LED elements can also be combined with filters to control the spectral emission of the LEDs and to evaluate luminescence.[23] Some proposals of multispectral systems using LED illumination and covering the visible range of the electromagnetic spectrum have been recently published[3,23–26]; these systems have been applied to measurements of cortical oxygenation,[23] microspectroscopic measurements in molecular multiplex assays,[25] and ocular fundus imaging.[3]

In artwork imaging, the use of LED irradiation in multispectral systems has the advantage of limiting light exposure to the target surface, a desirable characteristic for conservation purposes.[27] This technique can provide low acquisition times through fast switching and the possibility of irradiating extended areas; it can also be reliably operated in situ because of the compact approach that assembles radiant sources and acquisition into the system without mobile parts.

In this article, we report on the use of a LED-based multispectral system[28] for imaging of paintings. The system encompasses from 370 to 1630 nm, the spectral range capable of providing the most relevant information. We describe first the system setup and provide next a brief description of the methods used for spectral reconstruction as well as the metrics for performance evaluation. Some applications to the study of Catalan masterpieces are finally reported to demonstrate the potential of this technique.

METHODS AND MATERIALS

System Setup

To acquire spectral images in the 370 to 1630 nm spectral range, the imaging equipment featured two main parts or modules, each one comprising an imaging sensor and a spectral light source based on LEDs. These two parts are basically determined by the commercial availability, costs, and characteristics of the cameras. Unfortunately, there is no commercial camera capable of providing at the same time good spatial resolution and spectral sensitivity to work over part of the near-UV, visible, and near-IR to 1630 nm. This is particularly critical in the IR zone, where even with cameras dedicated to this spectral range, prices are too high and performance characteristics too low, among them the spatial resolution, in comparison with the silicon-based cameras for the visible range. Thus, in this system, a compromised solution using two sensors was adopted assuming a reasonable economical cost.

In this way, these two parts can be linked to its own spectral window, the first one (module 1) covering from 370 to 950 nm and the second (module 2) from 930 to 1630 nm. Module 1 consists of a cooled CCD monochrome camera (QICAM Fast 1394; Qimaging, Canada) with 12 bit depth of digitalization and a 1392 $\times$ 1040 pixels sensing area. We removed the near-IR filter of this camera to achieve a spectral response up to 950 nm. This camera is coupled to a lens (Cinegon Serie Compact 12 mm f/#1.4; Scheider-Kreuznach, Germany) with high transmittance between 400 and 1000 nm. The corresponding spectral light source has 16 channels that originate from different groups of LEDs (peak wavelengths of emission [in nm]: 373, 404, 432, 461, 500, 353, 593, 634, 665, 693, 728, 761, 801, 835, 874, and 903). For module 2, the imaging sensor is an InGaAs camera (C10633-13; HAMAMATSU, Japan) with 14 bit depth of digitalization and a 340 $\times$ 256 pixels sensing area. This camera uses a short-wave IR (SWIR) lens (LM12HC-SW 12.5 mm

Fig. 1. Experimental setup of the portable multispectral system.

f/#1.4; KOWA, Japan) with improved transmittance between 800 and 2000 nm. The spectral irradiation for this part of the SWIR spectral region is obtained with seven different groups of LEDs (peak wavelengths of emission [in nm]: 955, 1071, 1202, 1297, 1451, 1540, and 1630). In total, the system provides 23 spectral channels that originate from LED irradiation. The spectral channels provided by the radiant sources have full width at half maximums that range from 9.5 to 45 nm in module 1 and from 51 to 126 nm in module 2. The separations between emission peaks in module 1 are around 40 nm, whereas in module 2, they are above 90 nm. This wider separation between peaks of emission in the SWIR spectral region is caused by a more limited commercial availability for LEDs in this wavelength range.

The two LED sources in the system provide a fairly uniform irradiance field. To this end, each specific wavelength is generated by four LEDs arranged in a symmetrical way over a circular ring, with a separation of 90° between them (Fig. 1). In addition, the radiant source includes a diffusing filter in front of the LED elements to diminish the influence of their typical directional emission. This configuration enabled the corresponding camera to measure through the hole of the ring-like light source and to capture the spectral images, thus using diffuse irradiation and observation at 0° (d/0°). The system is mounted on a rail assembled to a tripod (Fig. 1) so that the system can be displaced laterally over the rail and vertically by changing the tripod height. Furthermore, the two corrected lenses, designed for each spectral range of the corresponding module, jointly with small apertures in the acquisition allowed to mitigate the effect of chromatic aberration over the spectral images. More details on this system can be found in Ref. 28.

Imaging Procedure, Spectral Recovery, and Performance Evaluation

A customized computational interface serves to control all the parameters of the system such as synchronization of image acquisition and LED emission; it also implements algorithms for noise correction, calibration, and processing of acquired information. The protocol to acquire the set of spectral images requires the sequential irradiation of the field of view (FoV) with the LED sources and the corresponding acquisition of 23 spectral images. This set of images can be understood as combined to form a three-dimensional (x, y, λ) spatial–spectral image cube, where x and y represent two spatial dimensions of the scene, and λ represents the spectral dimension. Each image of the cube is the result of averaging 10 frames to control the influence of temporal sources of noise, that is, irradiation sources and acquisition sensors.

The FoV of the system has been customized to the area of 25 cm × 25 cm of a white standard (BN-R98-SQ12: 98% reflective; Gigahertz-Optik, Germany). For this particular configuration, the equivalent projected area of the scene onto each pixel is of 180 μm × 180 μm for module 1 and 735 μm × 735 μm for module 2. With the use of this white standard, we have also set the parameters of offset, gain, and exposure time for all the channels of the system assuring the best use of the dynamic range of the cameras while working within the linear part of their responses. This means that the images are calibrated guaranteeing offset and maximum values around 4 and 95% of the maximum possible digital level for each camera, respectively.

We corrected the spatial nonuniformity for the response of the pixels of the camera and the irradiance field through a flat fielding process proposed by de Lasarte *et al.*,[29] based on capturing images of dark frames and of a uniform sample with calibrated reflectance. In this work, we have used the white standard panel used in image calibration that has uniform and high spectral reflectance over the range of 250–2500 nm. These dark and white standard images are captured under the parameters of offset, gain, and exposure time obtained for each channel in the calibration. This set of parameters is maintained to acquire the images of the samples, which jointly with the reflectance information of the white standard allow their interpretation as reflectance images when it is necessary.

Fig. 2. RGB image and the 23 spectral images of a section (zone 1) of the wall paintings in Saint Michael's chapel at the Royal Monastery of Saint Mary of Pedralbes (Ferrer Bassa).

To evaluate the spatial nonuniformity of the irradiance field and its correction, we used the spatial nonuniformity percentage (SNUP)[29] given by the following equation:

$$\mathrm{SNUP} = 100 \cdot \frac{\sigma(\bar{I})}{\bar{I}}, \tag{1}$$

where $\bar{I}$ represents the mean digital level of the image, and $\sigma(\bar{I})$ represents its associated standard deviation. We calculated SNUP values over the different channels of the system before the flat field correction and over a gray uniform sample. These values ranged from 4.83 to 10.66% and after correction they ranged from 0.07 to 0.33%, showing the good performance of the algorithm.

We used two widely known methods to recover spectral information. First, spline interpolation[30,31] that provides direct access to the spectrum of reflectance. The interpolation methods operate over the digital values in each spectral image, after the calibration, considering them as elements of a reflectance factor image, that is, as samples of the reflectance spectrum at the spectral channel wavelength. The accuracy of the interpolation methods is greatly dependent on the number of channels in the system. In this study, spline interpolation gives coarse but useful spectral information and does not require information on all system characteristics or prior knowledge of the samples to be imaged. Spline

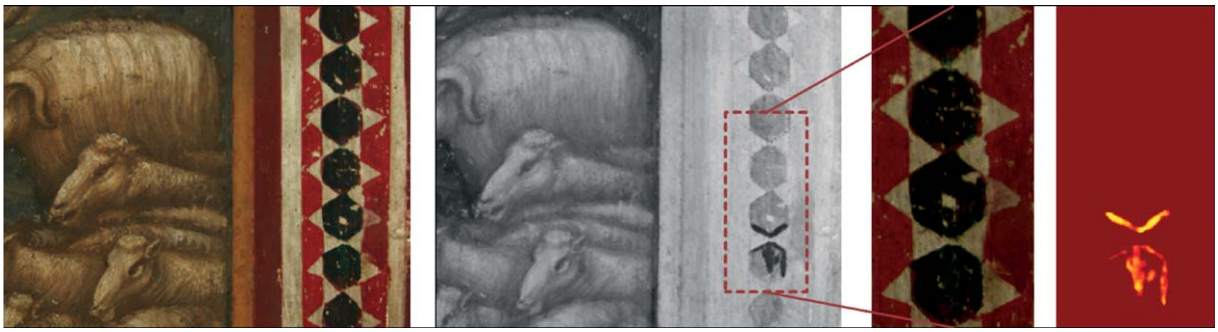

Fig. 3. RGB image, spectral image corresponding to 1202 nm, and a detail with the segmentation of the retouched section.

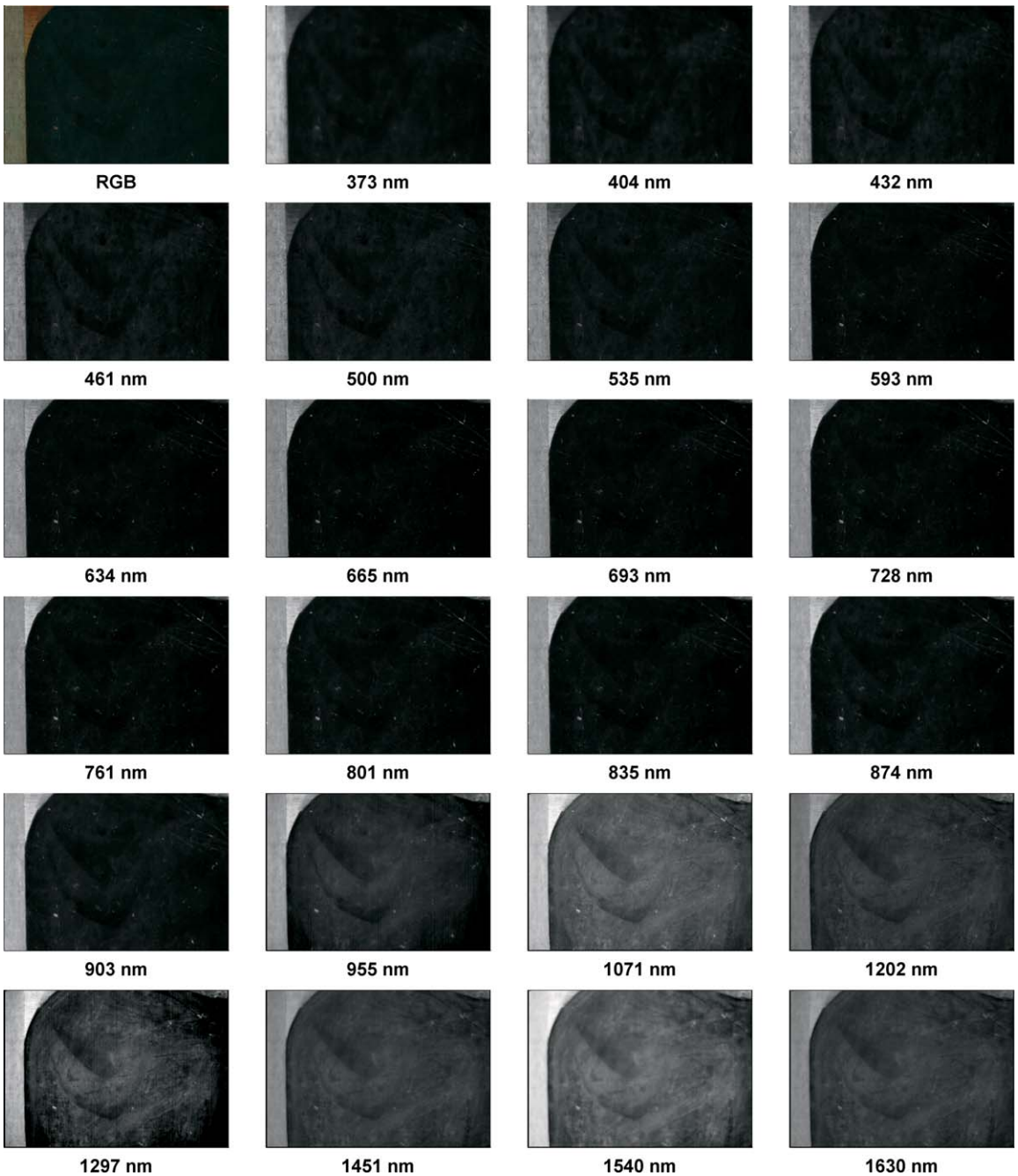

Fig. 4. RGB image and the 23 spectral images for a section (zone 2) of the wall paintings in Saint Michael's chapel at the Royal Monastery of Saint Mary of Pedralbes (Ferrer Bassa).

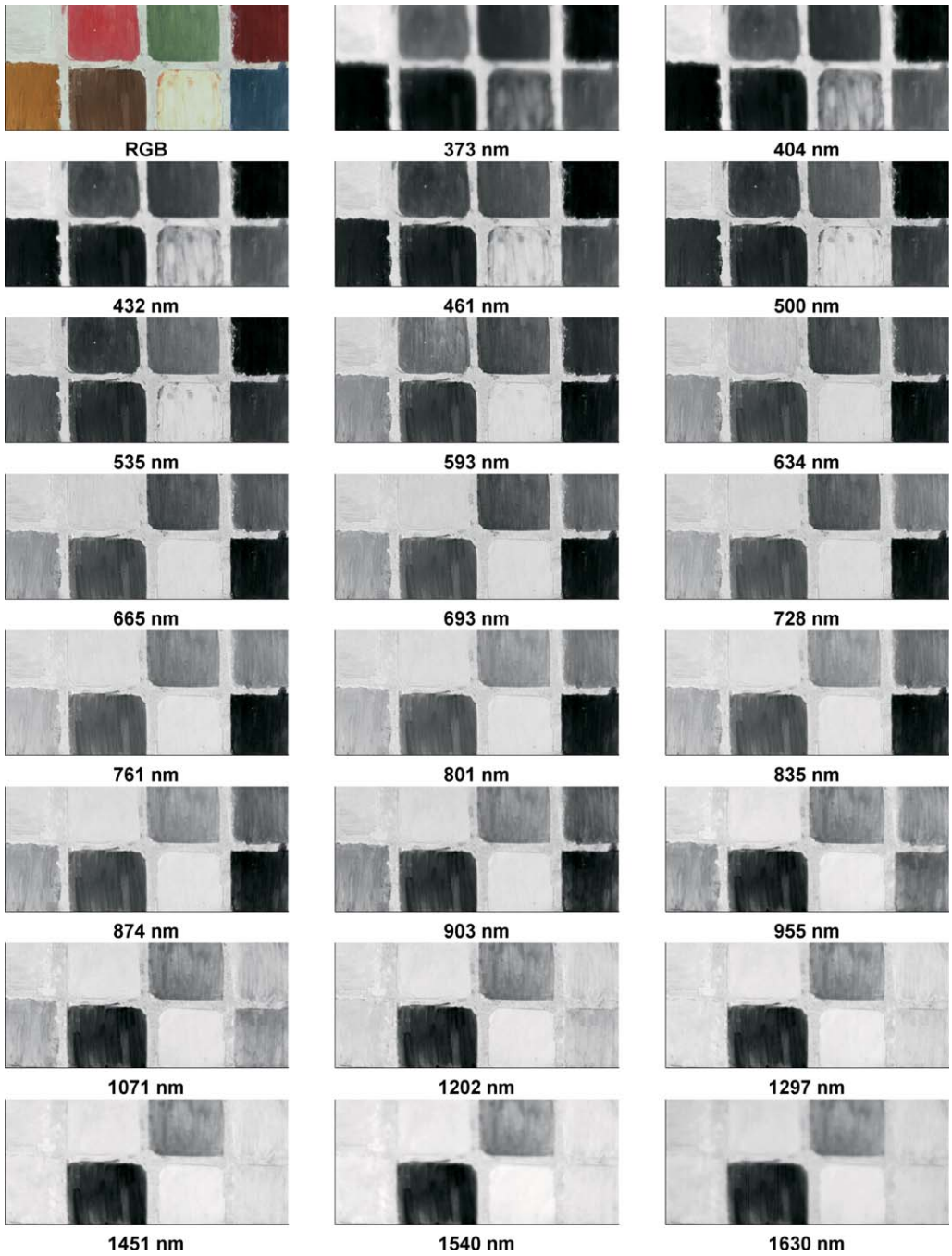

Fig. 5. One part of the palette of color patches (8) using pigments usually found in fresco paintings.

interpolation was specifically selected because its characteristic smoothness suits the expected type of spectral functions for real materials.

The pseudo-inverse method with training[15,32] was the second method of spectral reconstruction. This estimation method provides spectral reflectances from digital camera responses through a mapping matrix. This mapping matrix entails a pseudo-inverse procedure minimizing the least-square-error for the training dataset of known reflectances and corresponding camera responses. While this method generates good spectral results, it depends substantially on the distance between the set of training samples and the samples to capture.

Three different metrics were used to compare and evaluate the performance in the spectral reconstruction of the system. Two metrics compared the estimated spectral curves in relation to the reference spectra: the root mean square error (RMSE),[15,33] a widely used metric for spectral evaluation, and the goodness-of-fit coefficient (GFC) proposed by Hernández-Andrés *et al.*[33,34] This GFC is described by the following equation:

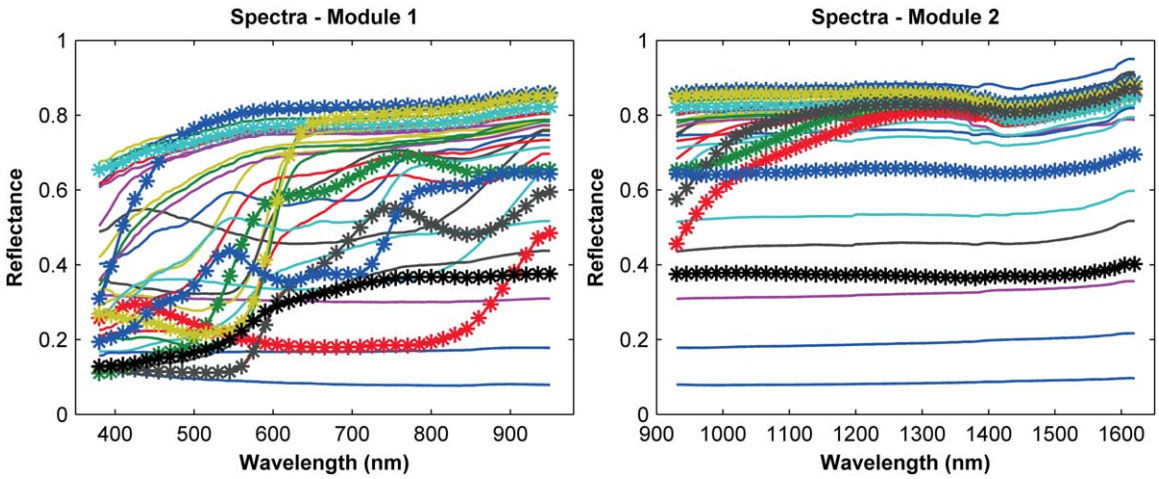

Fig. 6. Spectral reflectances from the palette of 32 patches for the training set generated using typical artwork pigments. Measurements carried out with a commercial spectrometer (Spectro 320 R5; Instruments Systems, Germany). The lines with star symbols correspond to the subset of patches shown in Fig. 5.

$$\mathrm{GFC} = \frac{\left|\sum_j r_o(\lambda_j) r(\lambda_j)\right|}{\left\{\sum_j [r_o(\lambda_j)]^2 \sum_j [r(\lambda_j)]^2\right\}^{1/2}}, \qquad (2)$$

where $r_o(\lambda_j)$ are the original spectral data at the wavelength λ_j and $r(\lambda_j)$ is the estimated spectrum at the wavelength λ_j. $\mathrm{GFC} \geq 0.995$, $\mathrm{GFC} \geq 0.999$, and $\mathrm{GFC} \geq 0.9999$ are required for acceptable, good, and excellent matches, respectively. The third metric is the CIEDE2000 formula (ΔE_{00})[35–37] used over the reconstructions in the visible range as a colorimetric evaluation. To compute the color data, the CIE D65 illuminant and CIE 1964-10 standard observer discretized at 5 nm wavelength intervals were used.

RESULTS OF ARTWORK IMAGING

We captured images at the Royal Monastery of Saint Mary of Pedralbes, Barcelona (http://www.bcn.cat/monestirpedralbes/es/). The images were acquired from the wall paintings by the painter Ferrer Bassa located in Saint Michael's chapel. These wall paintings are considered masterpieces of the 14th century Catalan Gothic art. We also imaged the anonymous diptych *The Nursing Madonna* (ca. 1500), an approximately 60 × 40 cm^2 oil on wood painting.

Imaging of Wall Paintings

Figure 2 contains the RGB and the 23 spectral images captured with the multispectral system for one section (zone 1) of the wall paintings in Saint Michael's chapel (the RGB image is the combination of the spectral images of 634, 535, and 461 nm for the R, G, and B channels, respectively). This set of images illustrates the captured information for each section of the mural. The examination of the images enables conservators and restorers to address features otherwise hidden in regular trichromatic imaging. By way of an example of the possibilities offered by the multispectral system and taking into account the scratches and degradation from aging, the hexagons in the images of Fig. 2 have uniform color in the spectral channels of the visible range. It could be therefore inferred that they were painted with the same material and have the same behavior over the whole spectral range covered by the multispectral system. Instead, as the spectral channels in the IR clearly show, there is a section that differs from the rest. It probably corresponds to the application of a retouch with a material different from the original.

Figure 3 shows a detail of the image with the possible restoration and the retouched area obtained with IR information. The area has been enhanced and segmented by a thresholding process over the images to help restorers.

Figure 4 shows another part of the mural paintings in Saint Michael's chapel (zone 2). In this case, the spectral images show more obvious strokes in the longer wavelengths than in the visible wavelengths, which are more affected by blackening due to aging and dirt. These findings may be of interest for the study of color aging and for the details of the original image and techniques used by the painter.

Additionally, spectral and accurate color information can be accessed from the spectral images by using interpolation or estimation methods. To access this information using the pseudo-inverse method, which requires a priori knowledge of the spectral samples to be measured, we used two training sets. The first set was a palette of 32 patches generated using the fresco technique and pigments usually found in this kind of wall paintings. These pigments correspond to colors like venetian red, red earth, green earth, burnt umber (brown), indigo, yellow, yellow ochre, and vegetal black (Figs. 5 and 6). For the second training set, we measured the spectral reflectance of 22 points over the wall paintings in Saint Michael's chapel with a commercial spectrometer (Spectro 320 R5; Instruments Systems, Germany). This set is also used in this

TABLE I. Results of evaluation metrics in spectral estimation for the set of selected sample points (22) over the wall paintings in Saint Michael's chapel.

	Module 1			Module 2	
Mean values	CIEDE2000	RMSE	GFC	RMSE	GFC
Interp	2.08	1.31	0.9995	2.60	0.9996
PSE (TrS: Pigments)	2.43	2.99	0.9987	4.90	0.9991
PSE (TrS: Wall points)	0.69	0.52	0.9999	2.51	0.9998

Interp, Spline Interpolation; PSE, pseudo-inverse; TrS, Training Set.

study as the test set for the performance evaluation of the system.

The patches in Fig. 5 are part of the complete set of pigments prepared as one of the training sets. Their corresponding spectra are depicted in Fig. 6 by the curves with the star symbols, together with the curves for the rest of the training samples belonging to this set. For example, the burnt umber pigment patch (second row, second column) that is dark in all the spectral images can be correlated with its corresponding spectral curve in Fig. 6, the black starred curve.

Table I shows the performance evaluation in spectral reconstruction for the sample points over the wall paintings in Saint Michael's chapel. The pseudo-inverse method with the sample points as training and test sets presents the best results. In this case, it could be inferred that some overfitting has taken place. The results for the spline interpolation method and the pseudo-inverse method using the palette of fresco patches as training set also show good results. However, the spline interpolation method presents better values, probably due to the smooth reflectance curves of the samples, and consequently the simpler fitting between the reference and interpolated spectral curves. Furthermore, the pseudo-inverse method can be influenced by the palette of pigments of the training set. The color differences under 2.5 units represent a good colorimetric reconstruction in all cases; RMSE and GFC show a good spectral fitting in module 1. Overall, module 2 presents a poorer performance than module 1 due to the lower number of spectral channels in this range.

Image Composition of Large-Sized Pieces

Another challenge typically found in artwork imaging is the capture of large-sized images such as frescos. Figure 7 shows the result of an image composition for the painting *The Nursing Madonn*a. This image was captured with the multispectral system through a sequence of movements and was later assembled from the set of subimages using a Matlab-based stitching algorithm derived from computing correlations of intersecting sections of individual images.

The painting in Fig. 7 shows some deterioration, for example, the vertical crack in the middle of the painting or the background color degradation. In these situations, the restorers and museum workers can use the detailed spatial information provided by the composed images of

Fig. 7. Result of the image composition for the painting *The Nursing Madonna* from a set of subimages acquired using the multispectral system (Painting from the Royal Monastery of Saint Mary of Pedralbes collection).

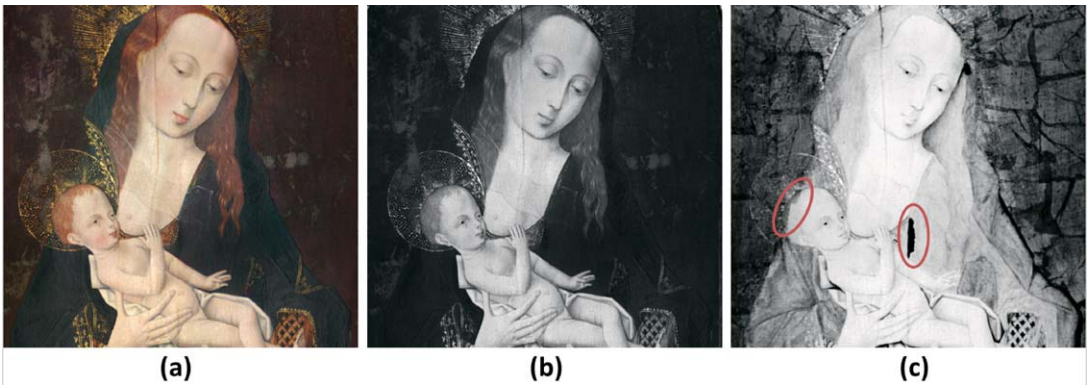

Fig. 8. Comparison of a section of the painting *The Nursing Madonna* to show the cracking of underlying layers of the painting: (a) RGB image; (b) spectral channel of 590 nm; and (c) spectral channel of 1202 nm enhanced through histogram equalization.

the system to assess the process over time. For example, Fig. 8 shows three images where a histogram equalization of the image corresponding to the spectral channel of 1202 nm [Fig. 8(c)] suffices to enhance and visualize the underlying layers where cracking of the materials are found. Additionally, other details from previous restorations not visible in the RGB image or the 590 nm spectral channel are also revealed, as highlighted in Fig. 8(c).

Apart from the specific image processing techniques we have presented here, several other novel algorithms may be implemented using these spectral data, and thus, even deeper insight on the samples can be obtained.

CONCLUSIONS

The information provided by the LED-based system shows the value of this technique in cultural heritage studies and artwork conservation. Features in the artworks hidden to plain sight or trichromatic imaging were revealed with this technique. The evaluation in spectral and colorimetric performance also showed that the system is a reliable tool for providing pixelwise reflectance information over a wide range of the spectrum. The composition of a large-sized artwork from a set of subimages was successfully achieved showing the versatility and suitability of the system in this kind of painting formats.

Because of the portability, compactness, modularity, and reliability, multispectral systems using LED technology constitute a cost-effective technique applicable to other areas of research. Furthermore, the combination and modification of the basic setup of this system with a wide range of other elements could have potential in applications such as luminescence evaluation, mottling/cloudiness evaluation in automotive coatings, performance of antigraffiti technologies, influence of UV-LED irradiance on artworks, plastic sorting systems, support in medical imaging, and diagnosis.

1. Giallorenzi TG. Optical technology in naval applications. Opt Photonics News 2000;11:24.
2. Weng Q, editor. Advances in Environmental Remote Sensing: Sensors, Algorithms, and Applications. Boca Raton: CRC Press; 2011. p. 610.
3. Everdell NL, Styles IB, Calcagni AS, Gibson J, Hebden JC, Claridge E. Multispectral imaging of the ocular fundus using light emitting diode illumination. Rev Sci Instrum 2010;81:093706.
4. Vilaseca M, Mercadal R, Pujol J, Arjona M, de Lasarte M, Huertas R, Melgosa M, Imai FH. Characterization of the human iris spectral reflectance with a multispectral imaging system. Appl Opt 2008;47:5622–5630.
5. Barbin DF, El Masry G, Sun D-W, Allen P. Predicting quality and sensory attributes of pork using near-infrared hyperspectral imaging. Anal Chim Acta 2012;719:30–42.
6. Wang XL, Waske B, Benediktsson J. Ensemble methods for spectral-spatial classification of urban hyperspectral data. 2009 IEEE International Geoscience and Remote Sensing Symposium, IGARSS 2009, Vol. 4. IEEE, Cape Town (Souh Africa). 2009. pp. IV–944. DOI: 10.1109/IGARSS.2009.5417534.
7. Lu R, Peng Y. Development of a multispectral imaging prototype for real-time detection of apple fruit firmness. Opt Eng 2007;46:123201.
8. Martínez-Verdú F, Chorro E, Perales E, Vilaseca M, Pujol J. Camera-based colour measurement. In: Gulrajani ML, editor. Colour Measurement: Principles, Advances and Industrial Applications. PA: Woodhead Publishing; 2010. pp. 147–166.
9. Barni M, Pelagotti A, Piva A. Image processing for the analysis and conservation of paintings: Opportunities and challenges. IEEE Signal Process Mag 2005;22:141–144.
10. Hardeberg JY, Schmitt F, Brettel H, Crettez JP, Maitre H. Multispectral image acquisition and simulation of illuminant changes. In L. W. MacDonald and R. Luo, eds, Colour Imaging: Vision and Technology. Chichester: John Wiley & Sons, 1999, pp. 145–164.
11. Redman J. Advances in digital imaging for fine art and cultural heritage. In: NIP23 and Digital Fabrication. Society for Imaging Science and Technology (IS&T), Springfield (USA) 2007. pp. 355–363.
12. Delaney JK, Zeibel JG, Thoury M, Littleton R, Palmer M, Morales KM, de la Rie ER, Hoenigswald A. Visible and infrared imaging spectroscopy of Picasso's Harlequin musician: Mapping and identification of artist materials in situ. Appl Spectrosc 2010;64:584–594.
13. Daffara C, Pampaloni E, Pezzati L, Barucci M, Fontana R. Scanning multispectral IR reflectography SMIRR: An advanced tool for art diagnostics. Acc Chem Res 2010;43:847–856.
14. Bonifazzi C, Carcagnì P, Fontana R, Greco M, Mastroianni M, Materazzi M, Pampaloni E, Pezzati L, Bencini D. A scanning device for VIS–NIR multispectral imaging of paintings. J Opt A: Pure Appl Opt 2008;10:064011.
15. Vilaseca M, Pujol J, Arjona M, de Lasarte M. Multispectral system for reflectance reconstruction in the near-infrared region. Appl Opt 2006; 45:4241–4253.
16. Berns RS. Multi-Channel Visible Spectrum Imaging, Digital Archiving and Reproduction. Rochester, NY; 2006. Available online at http://

msc.mellon.org/research-reports/Multi-Channel%20Visible%20Spectrum%20Imaging.pdf/view.

17. Ribés A, Schmitt F, Pillay R, Lahanier C, Ribes A. Calibration and spectral reconstruction for CRISATEL: An art painting multispectral acquisition system. J Imaging Sci Technol 2005;49:563–573.
18. Kong L, Yi D, Sprigle S, Wang F, Wang C, Liu F, Adibi A, Tummala R. Single sensor that outputs narrowband multispectral images. J Biomed Opt 2010;15:10502.
19. Mathews S. Design and fabrication of a low-cost, multispectral imaging system. Appl Opt 2008;47:F71–F76.
20. Basiri A, Nabili M, Mathews S, Libin A, Groah S, Noordmans HJ, Ramella-Roman JC. Use of a multi-spectral camera in the characterization of skin wounds. Opt Express 2010;18:3244.
21. Hardeberg JY, Schmitt F, Brettel H. Multispectral color image capture using a liquid crystal tunable filter. Opt Eng 2002;41:2532.
22. Tran CD. Principles, instrumentation, and applications of infrared multispectral imaging, an overview. Anal Lett 2005;38:735–752.
23. Bouchard MB, Chen BR, Burgess S, Hillman EMC. Ultra-fast multispectral optical imaging of cortical oxygenation, blood flow, and intracellular calcium dynamics. Opt Express 2009;17:15670–15678.
24. Fauch L, Nippolainen E, Kamshilin AA. Accuracy of the reflectance spectrum recovery in a light-emitting diode-based multispectral imaging system. Opt Eng 2012;51:053201.
25. Li J, Chan RKY. Toward a UV–visible–near-infrared hyperspectral imaging platform for fast multiplex reflection spectroscopy. Opt Lett 2010;35:3330–3332.
26. Brydegaard M, Merdasa A, Jayaweera H, Ålebring J, Svanberg S. Versatile multispectral microscope based on light emitting diodes. Rev Sci Instrum 2011;82:123106.
27. Paviotti A, Ratti F, Poletto L, Cortelazzo GM. Multispectral acquisition of large-sized pictorial surfaces. EURASIP J Image Video Process 2009;2009:1–17.
28. Herrera-Ramírez J, Vilaseca M, Pujol J. Portable multispectral imaging system based on light-emitting diodes for spectral recovery from 370 to 1630 nm. Appl Opt 2014;53:3131.
29. de Lasarte M, Pujol J, Arjona M, Vilaseca M. Optimized algorithm for the spatial nonuniformity correction of an imaging system based on a charge-coupled device color camera. Appl Opt 2007;46:167–174.
30. Andrews H. Cubic splines for image interpolation and digital filtering. IEEE Trans Acoust 1978;26:508–517.
31. Kiusalaas J. Numerical Methods in Engineering with MATLAB®. Cambridge: Cambridge University Press; 2005.
32. Shen H-L, Cai P-Q, Shao S-J, Xin JH. Reflectance reconstruction for multispectral imaging by adaptive Wiener estimation. Opt Express 2007;15:15545.
33. Imai FH, Rosen MR, Berns RS. Comparative study of metrics for spectral match quality. In Proceedings of the First European Conference on Colour in Graphics, Imaging and Vision. Springfield VA: IS&T, 2002. pp. 492–496.
34. Hernández-Andrés J, Romero J, Lee RL. Colorimetric and spectroradiometric characteristics of narrow-field-of-view clear skylight in Granada, Spain. J Opt Soc Am A Opt Image Sci Vis 2001;18:412–420.
35. Melgosa M, Trémeau A, Cui G. Colour difference evaluation. In: Fernandez-Maloigne C, editor. Advanced Color Image Processing and Analysis. New York: Springer; 2013. pp. 65–85.
36. Sharma G, Wu W, Dalal EN. The CIEDE2000 color-difference formula: Implementation notes, supplementary test data, and mathematical observations. Color Res Appl 2005;30:21–30.
37. Luo MR, Cui G, Rigg B. The development of the CIE 2000 colour-difference formula: CIEDE2000. Color Res Appl 2001;26:340–350.